Improved PWM Modulation for a Permanent-Split Capacitor Motor

E.R. Benedict, T.A. Lipo
Department of Electrical and Computer Engineering
University of Wisconsin-Madison
Madison, WI 53706 USA
Tel:(608)262-0287, Fax:(608)262-5559

Abstract—**This paper first examines and compares several methods for producing a variable speed drive for the permanent split-capacitor (PSC) induction motor. Conventional modulation methods are compared using phasor diagrams and then an improved modulation scheme using a boost converter and a three-phase drive is proposed. The derivation of the required excitation waveforms for any arbitrary PSC machine as a function of the turns ratio α is presented in addition to an expression for determining the amount of required DC Bus boost. Experimental and theoretical results are included to verify the analysis.**

I. Introduction

THE permanent-split capacitor (PSC) motor is widely used for consumer fixed-speed applications such as in residential HVAC blowers and compressors. Variable speed operation of this motor drive will potentially be able to save a great deal of energy and money for consumers [1] and thus, this is a current topic of research interest.

The PSC motor is usually a two-phase, asymetrically wound machine which is operated from a single-phase voltage source with a capacitor connected in series with one of the two windings (the auxiliary winding) as shown in Figure 1. The capacitor value is chosen so that the total impedance in the auxiliary winding (auxiliary winding impedance plus the external capacitance) produces a sufficient phase shift in the current so that a rotating MMF is developed inside of the machine. The rotating MMF is developed when the phase currents are in quadrature. The series connection of the capacitor and the inductive auxiliary winding effectively creates a resonant tank which raises the applied voltage across the auxiliary winding. In order to keep the MMF produced by this winding equal to that produced by the main winding, the auxiliary winding has additional turns, a greater resistance and a reduced current causing the PSC induction motor to be asymetrical [2]. Finally, the turns ratio, α, is defined to be

$$\alpha = \frac{V_{\text{aux}}}{V_{\text{main}}} \tag{1}$$

Because the total auxiliary winding impedance is sensitive to the excitation frequency, there is a narrow range of frequencies over which the machine can be operated efficiently with the specified capacitor. This necessitates changing the auxiliary winding capacitance for the different excitation frequencies. Methods which allow for a continuous adjustment of the auxiliary winding capacitance have been demonstrated [3], [4]; however, a variable frequency excitation source is still required. Replacing the series capacitor in the auxiliary winding with an inverter and varying the phase angle of the winding current while holding the frequency constant has also been studied in [5]. This method of speed control has pulsating torques, acoustic noise and excessive motor heating which consequently do not make it a viable option.

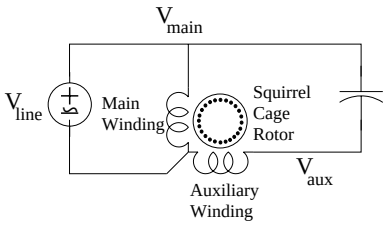

Fig. 1. Fixed Speed, Single-Phase Motor Circuit

A poly-phase, variable speed drive can be used to produce the required two-phase excitation directly without the capacitor and various topologies have been proposed and examined [6], [7], [8], [9], [10], [11]. In [6] two full-bridge single phase inverters are used, one for each winding. This has the simplicity of control and operation; however, it comes with a very high switch count. In [7], a three-phase bridge coupled with a standard rectifier is examined and in [8] a boost converter is included and a circuit diagram is shown in Figure 2. This circuit reduces the switch count from that in [6]. In [7], [11], [12], [13], [14] a further switch count reduction is proposed where the rectifier has a voltage doubling configuration and it is either uncontrolled [7], [12] or actively controlled [11], [13], [14]. The circuit for the actively controlled drive is shown in Figure 3. This topology provides a higher DC bus voltage while providing a reduced switch

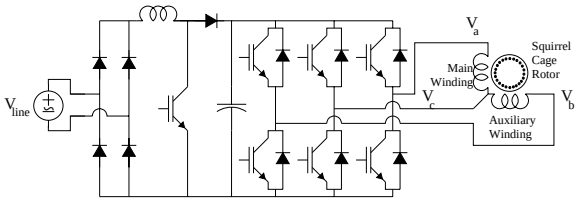

Fig. 2. Voltage Boost Two-Phase Variable Speed Drive

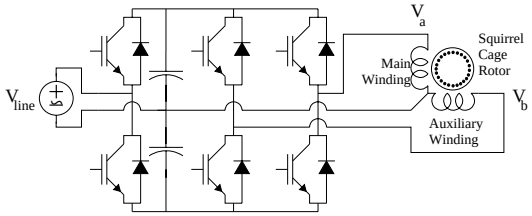

Fig. 3. Voltage Doubling Two-Phase Variable Speed Drive

count. The actively controlled topology also provides the benefit of input current shaping to provide a unity power factor as well as further increasing the DC bus voltage if the power factor correction is implemented [15].

Different modulation strategies for the inverters have been examined in recent literature. Sine-triangle PWM is studied in [10], [12]. In [9], [11], Space Vector PWM (SVPWM) is applied to a symmetrical machine. Also in [11], the SVPWM is extended to include asymmetrical two-phase machines by incorporating the turns-ratio α in the current command. Reference [11] reports that exciting an asymmetrical machine with a symmetrical voltage source produces oscillatory torque as expected.

In [10], Holmes and Kotsopoulos examine two different modulation strategies for the sine-triangle PWM of a three leg inverter. The first strategy examined is to hold the common terminal at the mid-point of the DC bus and then modulate the two remaining phases to achieve the following voltage set

$$\begin{aligned} V_a &= |V_{\text{main}}|\cos(\omega t) + \frac{V_{dc}}{2} \\ V_b &= |V_{\text{aux}}|\sin(\omega t) + \frac{V_{dc}}{2} \\ V_c &= \frac{V_{dc}}{2}. \end{aligned} \tag{2}$$

The vector diagram showing this modulation scheme is shown in Figure 4. The dotted circle represents the maximum

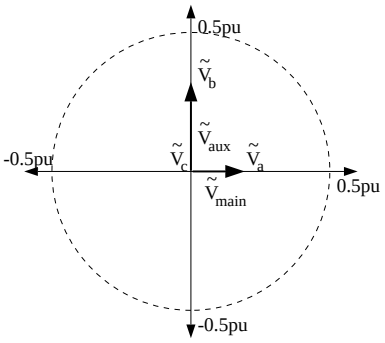

Fig. 4. Simple Modulation Voltage Phasor Diagram

output voltage which a single inverter leg is capable of producing. The per unit base, 1.0 pu, corresponds to the DC Bus voltage. From this figure, it is clear that for this modulation strategy, the peak obtainable voltage from a 1.0 pu DC bus is limited to 0.5 pu. The minimal switch count circuits of [7], [11], [12], [13], [14] all are subjected to this modulation limit; however, those with the boost capability can increase the DC bus as will be discussed.

Next, Holmes and Kotsopoulos consider a modulation strategy which is similar to the third harmonic injection technique. In this improved strategy, they inject a fixed common mode AC signal into each of the three phase legs to increase the peak obtainable voltage. The resulting phase voltages are

$$\begin{aligned} V_a &= |V_{\text{main}}|\cos(\omega t) + 0.5\cos(\omega t + \delta) + \frac{V_{dc}}{2} \\ V_b &= |V_{\text{aux}}|\sin(\omega t) + 0.5\cos(\omega t + \delta) + \frac{V_{dc}}{2} \\ V_c &= \frac{V_{dc}}{2} + 0.5\cos(\omega t + \delta) \end{aligned} \tag{3}$$

where

$$-\tan(\delta) = \frac{V_{\text{aux}}^{\max}}{V_{\text{main}}^{\max}}.$$

They show that for an equal turns ratio, $\alpha = 1.0$, the maximum output voltage where the quadrature relationship is possible is 0.707 pu. The phasor diagram for this modulation scheme is shown in Figure 5. Note that the phase voltages $\tilde{V}_a$, $\tilde{V}_b$ and $\tilde{V}_c$

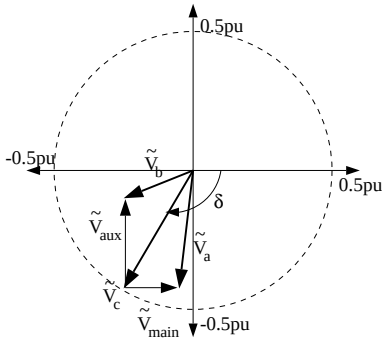

Fig. 5. Common-Mode Injection Modulation Scheme Voltage Phasor Diagram

are not equal in magnitude, except in the case where $|V_{\text{aux}}|$ is a maximum.

In [10], it is stated that the maximum $|V_{\text{aux}}|$ is 0.707 pu; however, this is correct only for unity α. Examination of Figure 5 shows that the maximum output voltage will be dependent on the winding turns ratio α and can be calculated using the Law of Cosines:

$$V_{\text{aux}}^{\max} = \sqrt{0.5 - 0.5\cos\left(2\tan^{-1}(\alpha)\right)} \tag{4}$$

The maximum output voltage while maintaining the quadrature relationship is plotted for different values of α in Figure 6.

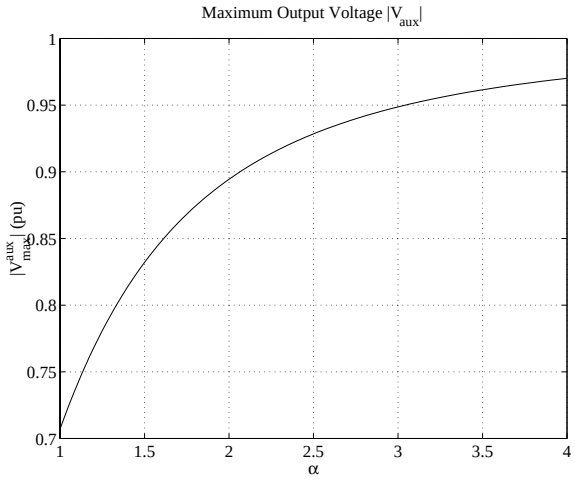

Fig. 6. Maximum Output Voltage

II. Proposed Modulation Strategy

As has been observed earlier [2], it is important that the main and auxiliary phase winding currents be maintained with a 90^o

phase relationship. If the winding impedances are assumed to have the same ratio between the resistance and reactance, then the winding currents will have the same relationship as the winding voltages. First the case where this assumption holds will be examined and then the results will be modified to handle the cases where the assumption is not true.

A. Simplified Case

The desired voltage relationship for geometrically similar winding impedances is illustrated by Figure 7.

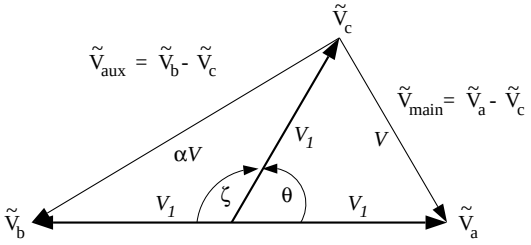

Fig. 7. Voltage Phasor Diagram

As a design constraint, it is proposed that all three inverter phase voltages, V_a, V_b and V_c, have the same amplitude, similar to that proposed by [6], [7], [8]

$$|V_a| = |V_b| = |V_c|.$$

This will make the voltage stress on all devices equal, improve the device utilization and provide the maximum possible output voltage for a given DC bus voltage. This assertion is shown in the Appendix. This constraint is incorporated in the phasor diagram of Figure 7 since each phasor has a length equal to V_1. Observation of the figure shows that the main and auxiliary winding voltages are simply

$$V_{\text{aux}} = V_b - V_c \qquad V_{\text{main}} = V_a - V_c$$

and that the ratio between the main winding voltage and the auxiliary winding voltage is α.

Performing basic trigonometry, θ can be found to be

$$\theta = 180^o - 2\tan^{-1}(\alpha) \tag{5}$$

and that V_1 is obtained by applying the Pythagorean Theorem. Solving for V_1,

$$V_1 = V\frac{\sqrt{1+\alpha^2}}{2}. \tag{6}$$

The phasor diagram for the proposed modulation scheme in a format similar to the earlier examined modulation schemes is shown in Figure 8.

Because the proposed modulation strategy at maximum output voltage becomes equivalent to (3), the $V_{\text{aux}}^{\max}$ limit of (4) is applicable. This means that the minimum required voltage boost can be determined so that full-rated operation of the machine is possible. This boost factor β is simply

$$\beta_{\text{Proposed}} = \frac{\alpha}{\sqrt{0.5 - 0.5\cos\left(2\tan^{-1}(\alpha)\right)}}. \tag{7}$$

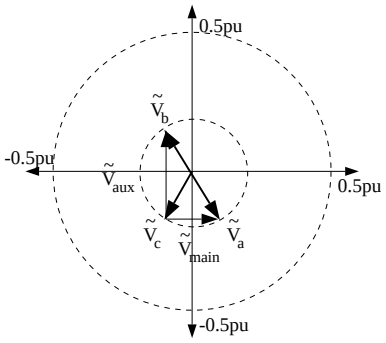

Fig. 8. Proposed Modulation Scheme Voltage Phasor Diagram

As a comparison, the β for the simple modulation is

$$\beta_{\text{Simple}} = 2\alpha. \tag{8}$$

Comparing (7) and (8) shows that the required boost for the proposed modulation strategy has a lower value than the simple modulation case. This indicates that the DC Bus voltage can be lower for the proposed modulation strategy. Depending on the turns ratio, this result suggests that the proposed strategy can use lower voltage rated switches which could offset the cost of the additional switches.

The proposed strategy can be implemented with many different formulations. In this paper, two specific formulations are proposed. The first one, (9), has a precomputed θ and V_1. This method is appropriate for applications where α is fixed and known at compile time.

$$\begin{aligned} V_a &= V_1\cos(\omega t) + \frac{V_{dc}}{2} \\ V_b &= -V_1\cos(\omega t) + \frac{V_{dc}}{2} \\ V_c &= V_1\cos(\omega t - \theta) + \frac{V_{dc}}{2}. \end{aligned} \tag{9}$$

The direction of rotation can be reversed by adding instead of subtracting θ. During run-time, this formulation requires only 2 multiplications, 4 additions and 2 table-lookups (for the cosine calcuations).

If the turns-ratio α must be computed during run time, then this formulation will require inverse trigonometric and square-root functions which does not make it desirable for run-time computation. A re-forming of the equations will result in (10) which is more suitable for applications where α must be adjustable at run time.

$$\begin{aligned} V_a &= \frac{1}{2}V_{\text{main}}\cos(\omega t) - \frac{1}{2}V_{\text{aux}}\sin(\omega t) + \frac{V_{dc}}{2} \\ V_b &= -\frac{1}{2}V_{\text{main}}\cos(\omega t) + \frac{1}{2}V_{\text{aux}}\sin(\omega t) + \frac{V_{dc}}{2} \\ V_c &= -\frac{1}{2}V_{\text{main}}\cos(\omega t) - \frac{1}{2}V_{\text{aux}}\sin(\omega t) + \frac{V_{dc}}{2} \end{aligned} \tag{10}$$

Here, the direction of rotation can be reversed by reversing the sign of the cosine terms. This formulation adds only two more additions and one multiplication over the precomputed θ formulation of (9).

B. Full Machine Model Case

When the assumption that the machine can be represented by two geometrically similar impedances is not sufficient, then the full machine model must be used in determining the required $V_{\rm main}$ and $V_{\rm aux}$ in order to obtain the required quadrature currents for constant torque production. In [5], analytic expressions for $V_{\rm main}$ and $V_{\rm aux}$ are developed in terms of the machine parameters and the machine's operating point (slip) so that the winding currents can have an arbitrary phase relationship. As has been mentioned earlier, having the winding currents in quadrature with their amplitudes scaled by α is the desired relationship.

The voltage phasor diagram for this case is shown in Figure 9. In this diagram, ϕ is the angle between the required main and

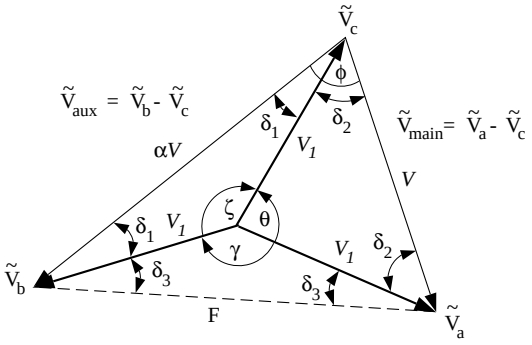

Fig. 9. Full Model Voltage Phasor Diagram

auxiliary winding voltages and α is the ratio between the voltage amplitudes as defined earlier.

Performing basic trigonometry,

$$\delta_3 = \frac{\pi}{2} - \phi$$

and so

$$V_1' = \frac{V}{2}\frac{\sqrt{\alpha^2 + 1 - 2\alpha\cos(\phi)}}{\cos(\frac{\pi}{2} - \Phi)} \tag{11}$$

From (11), δ_1 and δ_2 are found to be

$$\begin{aligned} \delta_1 &= \cos^{-1}\left[\frac{\alpha\cos(\frac{\pi}{2} - \phi)}{\sqrt{\alpha^2 + 1 - 2\alpha\cos(\phi)}}\right] \\ \delta_2 &= \cos^{-1}\left[\frac{\cos(\frac{\pi}{2} - \phi)}{\sqrt{\alpha^2 + 1 - 2\alpha\cos(\phi)}}\right]. \end{aligned}$$

Finally, the phase angles γ, θ and ζ are

$$\begin{aligned} \zeta &= \pi - 2\delta_1 \\ \theta &= \pi - 2\delta_2 \\ \gamma &= \pi - 2\delta_3 \end{aligned} \tag{12}$$

The three phase voltages, V_a, V_b and V_c can now be generated with

$$\begin{aligned} V_a &= V_1'\cos(\omega t) + \frac{V_{dc}}{2} \\ V_b &= V_1'\cos(\omega t - \gamma) + \frac{V_{dc}}{2} \\ V_c &= V_1'\cos(\omega t + \theta) + \frac{V_{dc}}{2}. \end{aligned} \tag{13}$$

This formulation will require 5 additions, 3 multiplications and 3 table-lookups which is a considerable increase in computational time over the simplified case.

III. Simulation Results

Theoretical computations of the inverter and motor phase voltages and motor phase currents from an ACSL simulation of the simplified case are shown in Figure 10 for the voltages and Figure 11 for the motor currents. The machine simulation

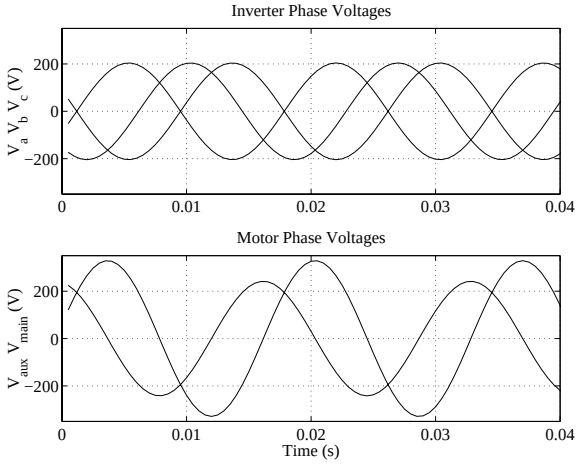

Fig. 10. Theoretical Inverter and Motor Phase Voltages

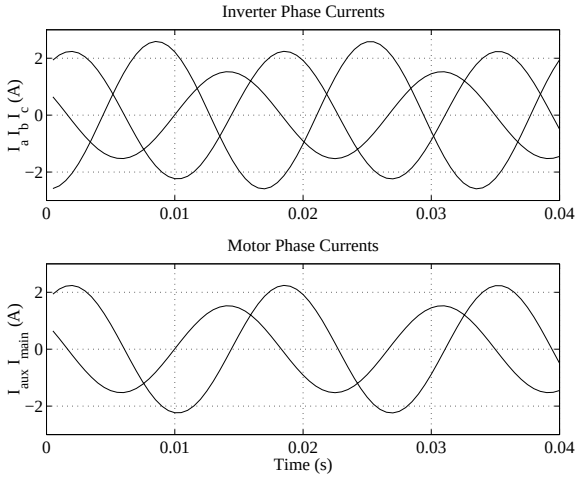

Fig. 11. Theoretical Inverter and Motor Phase Voltages

parameters are based on the 3/4 HP experimental machine described in Table I. The operating point was selected to be motor rated speed at the maximum output voltage of the experimental drive.

The motor winding currents can be plotted as a trajectory and when α is factored into the current, the scalled current trajectory represents the motor flux trajectory. These trajectories are shown in Figure 12. Examination of the current trajectory ellipse shows that the major axis of the ellipse is not perfectly horizontal which is expected because the simplified case was simulated. This results in the flux trajectory being a slightly distorted circle.

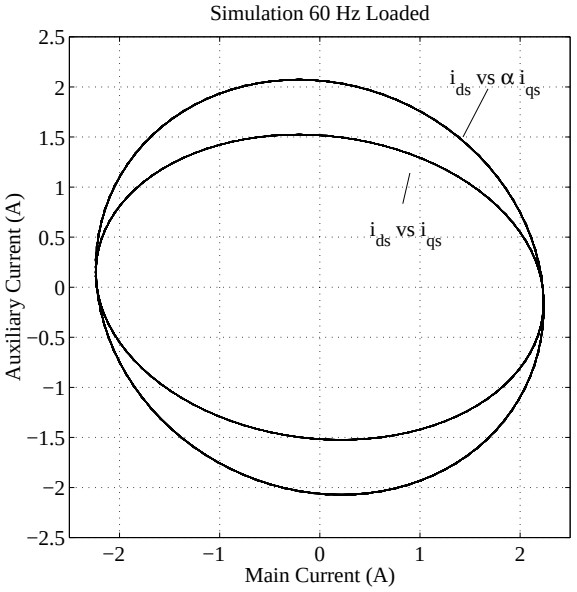

Fig. 12. Theoretical Current and Flux Trajectories

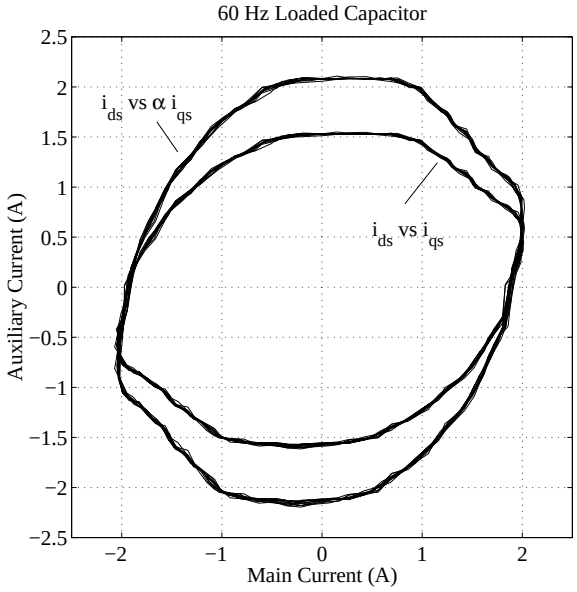

Fig. 13. Experimental Current for Capacitor Run Case

IV. Experimental Results

The drive of Fig 2 was constructed in hardware and the proposed strategy was implemented using a Microchip PIC17C756 microcontroller. This microcontroller was selected because of its low cost and the availablity of three independent hardware PWM timers, A/D inputs and a single-cycle multiplication. The constructed drive was used to operate a 3/4 HP PSC motor whose measured parameters are listed in Table I. All voltage and current measurements were recorded using a Fluke Model 41 Power Harmonics Analyzer. The operating point was selected so that at 60 Hz, the loaded machine had rated speed when operated from either the series capacitor or the drive.

TABLE I
6 Pole, 230V, 60Hz Motor Parameters

R_{1m}	8.69Ω	R_{1a}	21.8Ω
R_{2m}	9.91Ω	R_{2a}	20.8Ω
L_{1m}	32.8 mH	L_{1a}	60.7 mH
L_{2m}	32.8 mH	L_{2a}	60.7 mH
L_{Mm}	366 mH	L_{Ma}	677 mH
α	1.36	J_{rotor}	$1.407 \cdot 10^{-3}$ kg-m^2
ω_{rated}	1110 RPM	Power	3/4 HP

The current trajectory for the motor operating with the rated $10\,\mu$F capacitor in the auxiliary winding is shown in Figure 13. When the auxiliary winding current is scaled by the turns ratio, the current trajectory becomes more circular as expected.

The current trajectory for the motor operating with the drive at 60, 40 and 20 Hz are shown in Figures 14, 15, and 16 respectively. Trajectories for both the unscaled and scaled auxiliary winding current are overlaid in these figures. Comparison of the theoretical 60 Hz trajectories in Figure 12 and the experimental trajectories of Figure 14 show very good agreement.

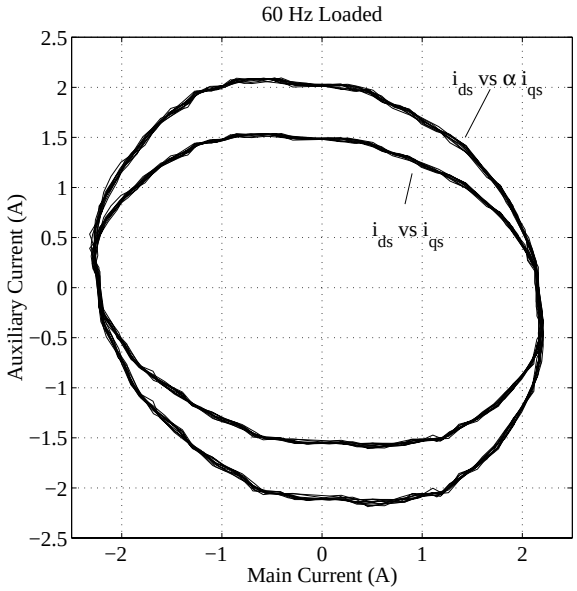

Fig. 14. Experimental Current for Drive at 60 Hz (Compare with Figure 12)

V. Conclusions

Different schemes for obtaining variable speed operation from a permanent-split capacitor motor have been examined and compared resulting in the proposal of an improved strategy. The strategy has been simulated and experimentally verified with very good agreement between the simulation and experiment.

This strategy does not use a miminal switch count; however for the incremental cost of the two additional switches, the voltage stress and bus capacitor ripple current are reduced from the minimal switch topology.

This proposed modulation scheme has several advantages over the common-mode injection modulation scheme. First, all three phases are producing equal voltages for all operating points. Second, the real-time calculation is simpler since two of

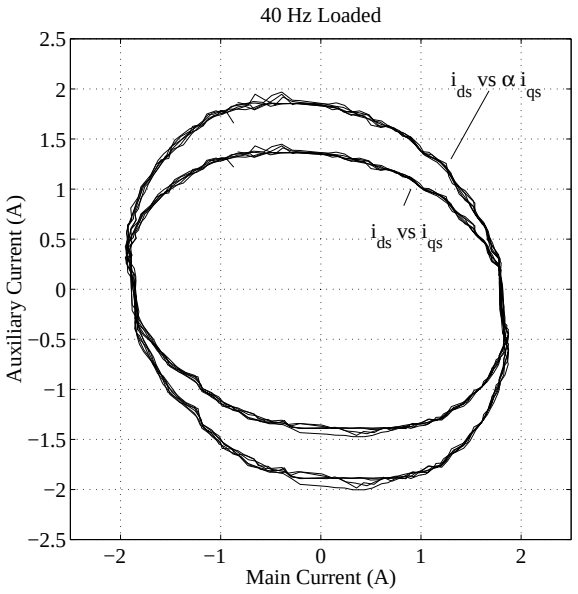

Fig. 15. Experimental Current for Drive at 40 Hz

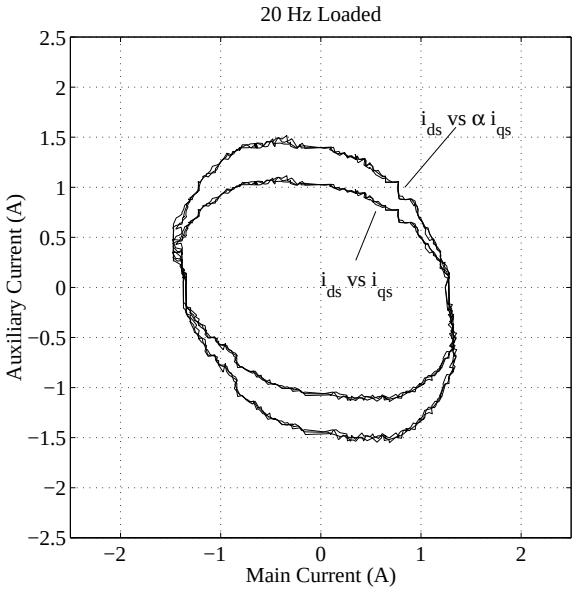

Fig. 16. Experimental Current for Drive at 20 Hz

the phases are always 180^o apart, so only a simple complementation is required to generate an additional phase. Third, only one sine and one cosine computation are required so the computation time is further reduced.

ACKNOWLEGEMENT

This work was performed as a part of the Center for Power Electronic Systems, CPES. CPES is an NSF Engineering Research Center (ERC). This ERC is supported by the NSF under Award Number EEC-9731677.

APPENDIX

I. PROOF OF MAXIMUM OUTPUT VOLTAGE STRATEGY

First, it will be shown that for a single frequency output voltage, the proposed strategy will produce the maximum output voltage. Then, it will be shown that the addition of harmonics will not produce a larger output voltage without introducing torque pulsations.

Because initially each phase voltage consists only of a sinusoid with a DC offset, each phase voltage can be represented as a phasor as in Figure 8. In this figure, the outer circle represents the maximum achievable voltage for each phasor.

If the motor winding voltages are represented as phasors then they will form a right triangle. Since the motor winding voltages are formed by the difference of the phase voltages as indicated by Figure 2, the verticies of the motor winding voltage triangle will be located by the phase voltage phasors.

In order to maximize the size of the triangle, it is clear that its verticies must be located on the outer circle. It can be shown through basic geometry that the hypotenuse of a circumscribing right triangle intersects the circle's center at the middle of the hypotenuse. This describes the proposed modulation strategy and shows that for the phasor case, the strategy produces the maximum voltage.

Now, assume that the phase voltages will be periodic with the operating frequency ω and that they are constructed from an N-term cosine Fourier series as

$$\begin{aligned} V_a' &= \sum_{i=0}^{N} a_i \cos(i\omega t + \phi_i^a) \\ V_b' &= \sum_{i=0}^{N} b_i \cos(i\omega t + \phi_i^b) \\ V_c' &= \sum_{i=0}^{N} c_i \cos(i\omega t + \phi_i^c) \end{aligned}$$

where

$$0 \le V_a', V_b', V_c' \le V_{\rm DC}\,.$$

If the DC component of V_a', V_b' and V_c' is fixed at $V_{\rm DC}/2$ then the Fourier series becomes

$$V_a' = V_a + \frac{V_{\rm DC}}{2} = \sum_{i=1}^{N} a_i \cos(i\omega t + \phi_i^a) + \frac{V_{\rm DC}}{2} \quad (14)$$

$$V_b' = V_b + \frac{V_{\rm DC}}{2} = \sum_{i=1}^{N} b_i \cos(i\omega t + \phi_i^b) + \frac{V_{\rm DC}}{2} \quad (15)$$

$$V_c' = V_c + \frac{V_{\rm DC}}{2} = \sum_{i=1}^{N} c_i \cos(i\omega t + \phi_i^c) + \frac{V_{\rm DC}}{2} \quad (16)$$

where

$$-\frac{V_{\rm DC}}{2} \le V_a, V_b, V_c \le \frac{V_{\rm DC}}{2}\,. \quad (17)$$

From Figure 2 and the required voltages for the PSC motor, the motor phase voltages will be

$$V_a - V_c = x\cos(\omega t) \quad (18)$$

$$V_b - V_c = \alpha x \sin(\omega t) \quad (19)$$

Subsituting (14), (15) and (16) into (18) and (19) results in

$$x\cos(\omega t) = \sum_{i=0}^{N}\left[a_i\cos(i\omega t+\phi_i^a) - c_i\cos(i\omega t+\phi_i^c)\right] \quad (20)$$

$$\alpha x\sin(\omega t) = \sum_{i=0}^{N}\left[b_i\cos(i\omega t+\phi_i^b) - c_i\cos(i\omega t+\phi_i^c)\right] \quad (21)$$

Because of the orthogonality of the cosine functions and the property of equality, the non-fundamental components ($i \neq 1$) all must be equal:

$$a_i\cos(i\omega t+\phi_i^a) = b_i\cos(i\omega t+\phi_i^b) = c_i\cos(i\omega t+\phi_i^c)\big|_{i\neq 1}\,.$$

For the DC component, $i = 0$, this requirement has been met with the assumption that the DC component is $V_{\rm DC}/2$.

After some algebra, this results in

$$\begin{aligned} V_a &= a_0 + a_1\cos(\omega t+\phi_1^a) + F(t) \\ V_b &= a_0 + a_1\cos(\omega t++\phi_1^a) + \alpha x\sin(\omega t) \\ &\quad -x\cos(\omega t) + F(t) \\ V_c &= a_0 + a_1\cos(\omega t+\phi_1^a) - x\cos(\omega t) + F(t) \end{aligned} \quad (22)$$

where

$$F(t) = \sum_{i=2}^{N} a_i\cos(i\omega t+\phi_i^a)$$

Observe that V_a, V_b and V_c must be between $-V_{\rm DC}/2$ and $V_{\rm DC}/2$ and that the addition of any harmonic other than triplens will result in increasing the peak amplitude of V_a, V_b and V_c. Therefore, $F(t)$ can only potentially contain triplen components.

An iterative Matlab program was written to determine the values of a_1 and ϕ_1^a with $F(t)$ as a third harmonic which maximizes x while observing the constraint of (17). The iterative program did not find any instances where a non-zero $F(t)$ increased x.

REFERENCES

[1] H. N. Hickok, "Adjustable speed — a tool for saving energy losses in pumps, fans, blowers, and compressors," *IEEE Transactions on Industry Applications*, vol. IA-21, pp. 124–136, January/February 1985.

[2] B. S. Guru and H. R. Hirziroğlu, *Electric Machinery and Transformers*. Harcourt Brace College Publishers, 2nd ed., 1995.

[3] E. Muljadi, Y. Zhao, T. H. Liu, and T. A. Lipo, "Adjustable ac capacitor for a single phase induction motor," in *IEEE/IAS Annual Meeting Conference Record*, pp. 185–190, IEEE Industry Applications Society, October 1991.

[4] T. A. Lettenmaier, D. W. Novotny, and T. A. Lipo, "Single-phase induction motor with an electronically controlled capacitor," *IEEE Transactions on Industry Applications*, vol. 27, pp. 38–43, January/February 1991.

[5] J. E. R. Collins, H. B. Püttgen, and I. W. E. Sayle, "Single-phase induction motor adjustable speed drive: Direct phase angle control of the auxilliary winding supply," in *IEEE/IAS Annual Meeting Conference Record*, pp. 246–252, IEEE Industry Applications Society, October 1988.

[6] F. E. Wills, H. R. Schnetzka, and R. D. Hoffer, "US Patent 5146147, AC motor drive system," 1992.

[7] F. E. Wills, H. R. Schnetzka, and R. D. Hoffer, "US Patent 5136216, AC motor drive system," 1992.

[8] F. E. Wills and H. R. Schnetzka, "US Patent 5218283, AC motor drive system with a two phase power supply," 1993.

[9] D.-H. Jang and D.-Y. Yoon, "Space vector pwm technique for two–phase inverter–fed single–phase induction motors," in *IEEE/IAS Annual Meeting Conference Record*, pp. 47–53, IEEE Industry Applications Society, October 1999.

[10] D. G. Holmes and A. Kotsopoulos, "Variable speed control of single and two phase induction motors using a three phase voltage source inverter," in *IEEE/IAS Annual Meeting Conference Record*, pp. 613–620, IEEE Industry Applications Society, October 1993.

[11] M. B. R. Correa, C. B. Jacobina, A. M. N. Lima, and E. R. C. da Silva, "Field oriented control of a single-phase induction motor drive," in *IEEE Power Electronics Specialists Conference Record*, pp. 990–996, IEEE Power Electronics Society, August 1998.

[12] C.-M. Young, C.-C. Liu, and C.-H. Liu, "New inverter-driven design and control method for two-phase induction motor drives," *IEE Proceedings — Electric Power Applications*, vol. 143, pp. 458–466, November 1996.

[13] M. F. Rahman, L. Zhong, and S. Y. R. Hui, "A single-phase, regenerative, variable speed induction motor drive with sinusoidal input current," in *EPE Conference*, vol. 3, pp. 777–780, IEEE Industry Applications Society, 1995.

[14] M. F. Rahman and L. Zhong, "A current-forced reversible rectifier fed single-phase variable speed induction motor drive," in *IEEE Power Electronics Specialists Conference Record*, pp. 114–119, IEEE Power Electronics Society, July 1996.

[15] P. N. Enjeti and A. Rahman, "A new single-phase to three-phase converter with active input current shaping for low cost AC motor drives," *IEEE Transactions on Industry Applications*, vol. 29, pp. 806–813, July/August 1993.